Langmuir
Article
pubs.acs.org/Langmuir

Effect of Cholesterol on Electrostatics in Lipid−Protein Films of a Pulmonary Surfactant

Eric Finot,[†] Yuri Leonenko,[‡] Brad Moores,[‡] Lukas Eng,[∥] Matthias Amrein,[⊥] and Zoya Leonenko*[,‡,§]

[†]*Institut Carnot de Bourgogne, University of Burgundy, Dijon, France,* [‡]*Department of Physics and Astronomy, and* [§]*Department of Biology, University of Waterloo, Canada,* [∥]*Institute of Applied Photophysics, Technical University Dresden, Germany, and* [⊥]*Department of Cell Biology and Anatomy, University of Calgary, Canada*

Received April 17, 2009. Revised Manuscript Received December 8, 2009

We report the changes in the electrical properties of the lipid−protein film of pulmonary surfactant produced by excess cholesterol. Pulmonary surfactant (PS) is a complex lipid−protein mixture that forms a molecular film at the interface of the lung's epithelia. The defined molecular arrangement of the lipids and proteins of the surfactant film gives rise to the locally highly variable electrical surface potential of the interface, which becomes considerably altered in the presence of cholesterol. With frequency modulation Kelvin probe force microscopy (FM-KPFM) and force measurements, complemented by theoretical analysis, we showed that excess cholesterol significantly changes the electric field around a PS film because of the presence of nanometer-sized electrostatic domains and affects the electrostatic interaction of an AFM probe with a PS film. These changes in the local electrical field would greatly alter the interaction of the surfactant film with charged species and would immediately impact the manner in which inhaled (often charged) airborne nanoparticles and fibers might interact with the lung interface.

Introduction

The air−lung interface is covered with a molecular film of pulmonary surfactant (PS). The PS film is a complex lipid−protein mixture primarily composed of lipids (75−80%) with small amounts of proteins (10%) and cholesterol (5−10% by mass). The major function of the film is to reduce the surface tension of the lung's air−liquid interface, providing stability to the alveolar structure and reducing the work of breathing. The PS film is also the first barrier in the body that nanosized particles (NSPs) in breathed air encounter. NSPs in the ambient (polluted) air pose a major health threat[1,2] and have been associated with substantial respiratory and cardiovascular morbidity and mortality[1−3] as well as cancer.[4,5] However, NSPs are prospective systems for aerosolized drug delivery to the lung. Both man-made and natural nanoparticles may be invariably charged[6] and may be affected strongly by electrostatic forces at the air−lung interface. For these reasons, understanding the electrostatic interactions of NSPs with PS films is of great importance. In this work, we investigated how the composition of a surfactant film and, in particular, excess cholesterol may affect these interactions through changes in the surface potential of the film. The apex of the AFM probe may serve as a model for the nanoparticle and therefore may provide important input into the interaction of nanoparticles with PS films. Cholesterol plays an important role in PS structure and function. We showed earlier that the function of pulmonary surfactant is greatly suppressed by excess cholesterol (20%), which has been associated with surfactant inhibition in adult respiratory distress syndrome.[7,8] We demonstrated earlier that excess cholesterol in PS films impairs surfactant function because of the prevention of multilayer formation, characteristic of normal functional surfactant[7] as a result of the loss of mechanical stability and reduced adhesion. In this work, we show that, in addition, excess cholesterol changes the local surface potential distribution of the PS film and alters the electrical potential in close proximity to the film, which affects the electrostatic interaction of the PS film with the AFM probe.

On a broader scale, the local electrical surface potential in a complex biomolecular monolayer such as PS is a direct reflection of its molecular-level structure and provides insight into the function of these films. Lipid monolayers are also widely used as models for studying biological membranes; therefore, our work may be helpful in elucidating the effect of cholesterol on the structure and function of biological membranes. Cholesterol plays an important role in controlling the fluidity, permeability, and mechanical strength of biological and model lipid membranes.[9−13] On the molecular scale, the incorporation of cholesterol into the membrane leads to an increase in lipid hydrocarbon

*Corresponding author. E-mail: zleonenk@uwaterloo.ca. Tel: (519) 888-4567, ext 38273. Fax: (519) 746-8115.

(1) Schwartz, J. F.; Laden, F.; Zanobetti, A. *Environ. Health Perspect.* **2002**, *110*, 1025–1029.
(2) Boldo, E.; Medina, S.; LeTertre, A.; Hurley, F.; Mucke, H. G.; Ballester, F.; Aguilera, I.; Eilstein, D. *Eur. J. Epidemiol.* **2006**, *21*, 449–458.
(3) Li, Z.; Carter, J. D.; Dailey, L. A.; Huang, Y. C. *Environ. Health Perspect.* **2005**, *113*, 1009–1014.
(4) Knaapen, A. M.; Borm, P. J. A.; Albrecht, C.; Schins, R. P. F. *Int. J. Cancer* **2004**, *109*, 799–809.
(5) Forastiere, F. *Occup. Environ. Med.* **2004**, *61*, 797–798.
(6) Bailey, A. G. *J. Electrost.* **1998**, *44*, 3–10.
(7) Leonenko, Z.; Gill, S.; Baoukina, S.; Monticelli, L.; Doehner, J.; Gunasekara, L.; Felderer, F.; Rodenstein, M.; Eng, L. M.; Amrein, M. *Biophys. J.* **2007**, *93*, 674–683.
(8) Gunasekara, L.; Schurch, S.; Schoel, W. M.; Nag, K.; Leonenko, Z.; Haufs, M.; Amrein, M. *Biochim. Biophys. Acta* **2005**, *1737*, 27–35.
(9) Demel, R. A.; Kruyff, B. D. *Biochim. Biophys. Acta* **1976**, *457*, 109–132.
(10) Ohvo-Rekilä, H.; Ramstedt, B.; Leppimäki, P.; Slotte, J. P. *Prog. Lipid Res.* **2002**, *41*, 66–97.
(11) McMullen, T. P. W.; Lewis, R. N. A.; McElhaney, R. N. *Curr. Opin. Colloid Interface Sci.* **2004**, *8*, 459–468.
(12) Bonn, M.; Roke, S.; Berg, O.; Juurlink, L. B. F.; Stamouli, A.; Muller, M. *J. Phys. Chem. B* **2004**, *108*, 19083–19085.
(13) Cadenhead, G.A. *Structure and Properties of Cell Membranes*; CRC Press: Boca Raton, FL, 1985.

chain order, the so-called condensation effect.[14−18] On the macroscale, cholesterol has a dual effect on membrane fluidity by broadening and eventually eliminating the liquid-to-solid phase transition of phospholipid membranes. Phase separation of phospholipid monolayers in the presence of cholesterol has been visualized by atomic force microscopy.[19] We hope that our findings on the effect of cholesterol in pulmonary surfactant may aid in the understanding of the role of cholesterol in the electrical properties of lipid monolayers and membranes. To the best of our knowledge, there were no experimental data reported so far on the local nanoscale electrostatic effect of cholesterol on the electrostatic interactions between an AFM probe and PS film.

Materials and Methods

Sample Preparation. In this work, we used pulmonary surfactant BLES (bovine lipid extract surfactant), which is a hydrophobic extract of bovine lung lavage that differs from natural surfactant in the lack of surfactant-specific proteins SP-A and SP-D and cholesterol. Pulmonary surfactant BLES is a lipid−protein mixture where phosphatidylcholines (PC) represent 80% of its mass with half of the PC being disaturated dipalmitoylphosphatidylcholine (DPPC). Five to ten mass % is the concentration of negatively charged phosphatidylglycerol (PG) and two hydrophobic surfactant-associated proteins (SP-B, SP-C). BLES in nonbuffered normal saline (pH 5 to 6) with a phospholipid concentration of 27 mg/mL was a kind gift from the manufacturer (BLES Biochemical Inc. of London, Ontario, Canada). Cholesterol was purchased from Sigma Chemicals (St. Louis, MO). To add cholesterol, a solution of 1:1:1 methanol/chloroform/BLES by volume was first vortex mixed and then spun in a centrifuge at 100G for 5 min. The methanol/water phase was discarded, and the BLES in chloroform was retained and either 0 or 20% cholesterol (by mass) with respect to phospholipids in chloroform was added. Each solution was then dried under N_2 and resuspended with Goerke's buffer (140 mM NaCl, 10 mM Hepes, and 2.5 mM $CaCl_2$; pH 6.9) or chloroform to obtain a solution of BLES at a concentration of 27 mg/mL phospholipids containing 0 or 20% cholesterol.

Atomic Force Microscopy and Force Measurements. For imaging and force measurements, BLES films were deposited onto a mica substrate by means of a Langmuir−Blodgett technique from buffer or chloroform solution. Freshly cleaved ASTMV-2 quality, scratch-free ruby mica (Asheville-Schoonmaker Mica Co., Newport News, VA) was used as a substrate. AFM morphology images of supported BLES films were collected in air with atomic force microscopy (NanoWizard AFM, JPK Instruments AG, Berlin) prior to force measurements. Silicon cantilevers from MikroMasch with a cantilever spring constant of 0.6 to 0.7 N/m (determined by a thermofluctuation method using JPK SPM software) and a resonance frequency of 41 kHz were used for imaging and following force measurements. To measure force versus distance plots, the atomic force microscope was used as a force apparatus. We performed force measurements on BLES films supported on mica in air. In an AFM force measurement, cantilever deflection Z_c is measured as a function of the distance between the scanner and the sample Z_p. Raw data (Z_c vs Z_p) were then converted into force F versus surface−tip separation D using Hooke's law, $F = k_s Z_c$, where k_s is the spring constant of the cantilever and the geometric relationship $D = Z_c - Z_p$ is for incremental changes.[20,21] All measurements were performed at 25 °C at five different velocities, collecting 10 force curves each time. To address the electrostatic interactions, we analyzed the approach part of the curve where the probe was brought into close proximity to the sample surface. The force plots were averaged and fit with theoretical models.

Frequency Modulation Kelvin Probe Force Microscopy. Surface potential images were obtained by frequency modulation Kelvin probe force microscopy (FM-KPFM[22]). Kelvin probe force microscopy (KPFM) is an AFM-based microscopy technique that is used to measure the local distribution of contact potential difference (CPD). The CPD is in turn a measure of the electrical surface potential or work function of the sample. KPFM is carried out by applying a voltage to a conducting AFM probe. Scanning the probe across the sample surface produces a map of the electrostatic interactions at each point on the sample. Commonly used KPFM methods, such as "lift mode",[22−24] have significant disadvantages. These include low resolution, low sensitivity, and an inability to perform AFM and KPFM imaging simultaneously. Moreover, the resolution and performance of KPFM methods are greatly affected by the environment.[22] As a result, for a long time KPFM methods had limited or no applications in biological research, which requires high resolution and high sensitivity because of very low electrostatic signals and an ambient environment. Frequency-modulated KPFM (FM-KPFM) overcomes these deficiencies[22,25] and is realized by applying ac voltage A_{mod} at the modulation frequency f_{mod} to a conducting AFM probe that is kept oscillating at its mechanical resonance frequency f_o close to the sample surface in noncontact mode. The principle of FM-KPFM used in this work and its capabilities were described by us in detail previously.[22,26] Briefly, the cantilever is forced to oscillate at f_o and f_{mod}, which superpose to produce side bands at $f_o \pm f_{mod}$. FM-KPFM overcomes all of the disadvantages of other Kelvin setups by tracking the electrostatic signal of interest at these side bands $f_o \pm f_{mod}$.[22] These side bands in FM-KPFM are very sensitive to the electrostatic forces because the carrier frequency f_o can be chosen out of noise bands or other disturbing resonances. Moreover, because FM-KPFM records the force gradient rather than the electrostatic force,[22,23,25] the largest sensitivity stems from the tip apex itself, avoiding any contribution from the tip shaft and cantilever beam that reflect the dc components in the Kelvin signal, commonly used in a lift-mode KPFM.[24] FM-KPFM allows the simultaneous recording of topographic and local surface potential images with very high resolution and sensitivity, reaching quantitative values even below the 1 nm resolution limit,[22] and is less affected by humidity. We demonstrated earlier its superior resolution of ∼1 nm and sensitivity of ∼1 mV in vacuum over other KPFM methods in imaging the work function in metallic and inorganic surfaces in vacuum.[22] We adapted a FM-KPFM method to map the local electric surface potential of pulmonary surfactant (PS) films in ambient air and demonstrated its superior resolution when compared to that of other modes.[26]

FM-KPFM mode images were collected using a homebuilt setup developed at Dresden University of Technology, which was described previously by Zerweck et al.[22] It comprises a homebuilt AFM, operated in noncontact mode using a homebuilt PLL, with the addition of Scientific Instruments SR830 and SR844 lock-in models. Conductive chromium/platinum tips were used for imaging. Constant tip−sample separation was controlled using a digital phase-locked loop (PLL) by maintaining a constant frequency shift during scanning and, constant phase difference

(14) Moy, V. T.; Keller, D. J.; Gaub, H. E.; McConnell, H. M. *J. Phys. Chem.* **1986**, *90*, 3198–3202.
(15) Weis, R. M.; McConnell, H. M. *J. Phys. Chem.* **1985**, *89*, 4453–4459.
(16) Subramaniam, S.; McConnell, H. M. *J. Phys. Chem.* **1987**, *91*, 1715–1718.
(17) Slotte, J. P. *Biochim. Biophys. Acta* **1995**, *1238*, 118–126.
(18) Worthman, L. A.; Nag, K.; Davis, P. J.; Keough, K. M. *Biophys. J.* **1997**, *72*, 2569–2580.
(19) Yuan, C.; Johnston, L. *J. Microsc.* **2002**, *205*, 136–146.
(20) Cappella, B.; Dietler, G. *Surf. Sci. Rep.* **1999**, *1*, 1–104.
(21) Butt, H. J.; Cappella, B.; Kappl, M. *Surf. Sci. Rep.* **2005**, *59*, 1–152.
(22) Zerweck, U.; Loppacher, C.; Otto, T.; Grafström, S.; Eng, L. M. *Phys. Rev. B* **2005**, *71*, 125424.
(23) Jacobs, H. O.; Leuchtmann, P.; Homan, O. J.; Stemmer, A. *Appl. Phys. Lett.* **1998**, *84*, 1168–1173.
(24) Charrier, D. S. H.; Kemerink, M.; Smalbrugge, B. E.; de Vries, T.; Janssen, R. A. J. *Nano* **2008**, *2*, 622–626.
(25) Kitamura, S.; Iwatsuki, M. *Appl. Phys. Lett.* **1998**, *72*, 3154–3156.
(26) Moores, B.; Eng, L. M.; Leonenko, Z. *Ultramicrosc. J.*, accepted for publication.

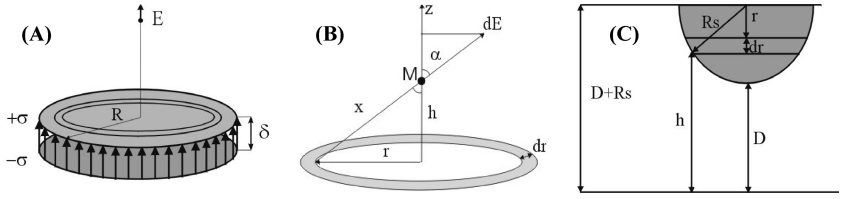

Figure 1. Electric field E induced by the lipid domain at the apex of the AFM tip. (A) A single domain composed of lipid molecules. The domain (or patch) can be considered to be two-plane disks with radius R and surface charge densities of $+\sigma$ and $-\sigma$ and separated by a distance δ, which corresponds to the thickness of the monolayer. (B) Electric field dE induced by a ring of radius r and width dr. (C) Modeling of the AFM tip as a semisphere.

between tip excitation and detected resonance. Image analysis was carried out using unfiltered FM-KPFM images, and potential differences were determined using cross-section analysis by averaging at least 50 measurements.

Modeling Electrostatic Interactions. To analyze experimentally measured forces, we developed theoretical models to fit the force plots. To account for the nonuniform surface potential distribution that we observed by KPFM, we introduced the patches (or domains) of various radii and surface potentials. To analyze electrostatic tip-patch interactions measured between an AFM tip and the film, we considered the AFM tip to be (1) a point charge, $Q_{tip} = Q_p$ and (2) a semisphere (with the charge $Q_{tip} = Q_s$ uniformly distributed on tip the surface). To account for nonuniform electrostatic domains, we modeled first the interaction of the AFM tip with the closest single domain below the tip. This domain is considered to be a round patch of radius R consisting of oriented electric dipoles (Figure 1A). The multiple domains around the central one were also considered and are described later.

Electric Field Induced by the Patch. The electric field dE of a single disk at any point M (Figure 1B) on the axis induced by the charge dq of a ring of radius r and width dr is given by

$$dE = k\frac{dq}{x^2} \tag{1}$$

where $k = 8.988 \times 10^9$ Nm^2/C^2 is the electrostatic constant and x is the distance between the charge $dq = 2\pi r\sigma\, dr$ and point M (Figure 1B). Because of the symmetry, only the z component dE_z of dE, dE_z = dE cos(α), contributes to the electric field. If M is at a vertical distance h, then we can rewrite eq 1 as

$$dE_z = k\frac{2\pi\sigma h r}{(r^2+h^2)^{3/2}}\, dr \tag{2}$$

The electric field E_z is found by integrating eq 2 over the disk radius:

$$E_z = 2\pi k\sigma h\int_0^R \frac{r\, dr}{(r^2+h^2)^{3/2}} = 2\pi k\sigma\left[1-\frac{1}{\sqrt{1+(R/h)^2}}\right] \tag{3}$$

The electric field E as a function of h (distance to the upper disk) induced by the patch is found as a superposition of the electric fields, produced by two disks separated by δ

$$E(h) = \frac{V}{2\delta}\left[\frac{1}{\sqrt{1+(R/(h+\delta))^2}}-\frac{1}{\sqrt{1+(R/h)^2}}\right] \tag{4}$$

where $V = 4\pi k\sigma\delta$ is the relationship between the surface charge density σ and surface potential V, assuming that the electric field between two parallel disks is equal to $4\pi k\sigma$ (as for two infinite planes). Surface potential V is taken from the measurements obtained by FM-KPFM.

Force Induced by the Patch on the AFM Tip. Using eq 4 for the electric field, we can calculate the force of interaction by considering the AFM tip to be a point charge and a semisphere.

Point Charge Model. In the case of a point charge, the electrostatic force F_p acting on Q_p as a function of distance D ($h = D$) is given by

$$F_p(D) = EQ_{tip} = \frac{VQ_p}{2\delta}\left[\frac{\beta}{\sqrt{1+\beta^2}}-\frac{\alpha}{\sqrt{1+\alpha^2}}\right] \tag{5}$$

where $\alpha = D/R$ and $\beta = (D+\delta)/R$ are dimensionless parameters.

Semisphere Model. When modeling the AFM tip as a semisphere (Figure 1C), we assume that the tip radius R_S is much smaller than the patch radius R.

The charge dq_s on the sphere ring dr can then be considered to be close enough to the axis of the patch so that eq 4 can be applied, assuming h to be the distance between dq_s and the patch. One can see (Figure 1C) that $h = D + R_s - r$, where R_s is the tip radius, D is the distance between the tip apex and the patch, and r is the radial coordinate with the origin at the center of the tip. As a result, we can obtain the expression for the electric field E as a function of r:

$$E(r) = \frac{V}{2\delta}\left[\frac{1}{\sqrt{1+(R/(D+R_s-r+\delta))^2}} - \frac{1}{\sqrt{1+(R/(D+R_s-r))^2}}\right] \tag{6}$$

The electric force dF between the patch and dq_s (charge of the sphere segment within dr) is d$F = E(r)$ dq_s. Assuming the uniform charge distribution of Q_s over the surface of the semisphere, the surface charge of the semisphere is given by $\sigma_S = Q_s/2\pi R_s^2$ and $dq_s = 2\pi R_s\sigma_s\, dr$ and the electrostatic force F_s between the patch and the semisphere tip can be found from

$$F_s = \int_0^{R_s} E(r)\, dq_s = \frac{Q_s}{R_s}\int_0^{R_s} E(r)\, dr \tag{7}$$

After integration,

$$F_s(D) = \frac{VQ_s}{2\delta\gamma}\left[\sqrt{1+\alpha^2}-\sqrt{1+\beta^2} + \sqrt{1+(\beta+\gamma)^2}-\sqrt{1+(\alpha+\gamma)^2}\right] \tag{8}$$

where $\alpha = D/R$, $\beta = (D+\delta)/R$, $\gamma = R_s/R$ are dimensionless parameters.

Multibody Interaction Model. The approach describing an isolated patch assumes that the neighboring patches have little or no influence on the force acting between the tip and the central patch. However, when the surface potential is not uniform, the

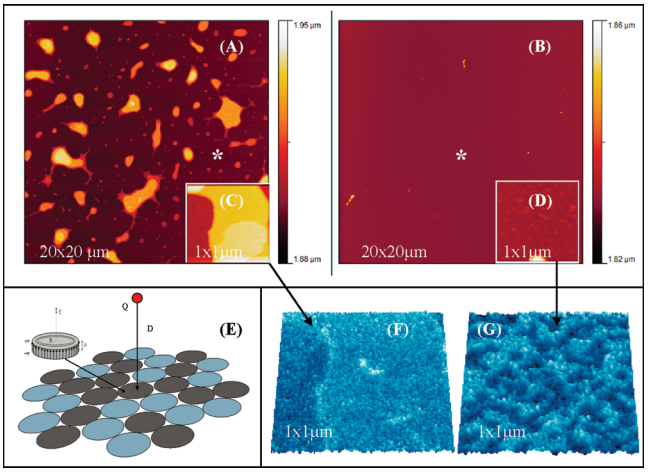

Figure 2. (A) AFM topography image of a surfactant film with 0% cholesterol. (B) AFM topography image of a surfactant film with 20% cholesterol. (C) Small AFM topography scan of a surfactant film with 0% cholesterol. (D) Small AFM topography scan of a surfactant film with 20% cholesterol. (E) Schematic representation of electrostatic domains, produced by cholesterol, interacting with the AFM probe. (F) FM-KPFM image of a surfactant film with 0% cholesterol (correlating topography shown in the inset of C). (G) FM-KPFM image of a surfactant film with 20% cholesterol (correlating topography shown in the inset of D). Asterisks show typical monolayer areas where the force curves were collected.

interaction between the tip and multiple domains should be considered. To take this into account, we developed a multibody interaction model where the tip was considered to be a point charge (or a semisphere) and the surface was viewed as an organized structure composed of N circular patches having two different surface potentials as obtained experimentally by KPFM measurements (Figure 2E). The tip is assumed to be above the center of one patch, interacting with N patches, each separated from the tip by a distance D_j, all having the same radius R. Blue (B) and gray (G) disks (Figure 2E) represent electrostatic domains having two different electric surface potentials, (−0.35 and −0.45 V), observed by FM-KPFM. The first disk (gray) is positioned in the center, right below the tip, and other disks are placed around and their positions are described by the radius from the center R_c. Four circles were considered at distances of $R_{cj} = 2R$, $3.33R$, $4R$, and $5.9R$ from the central disk. It was shown that other disks placed at $R_{cj} = 5.9R$ do not significantly alter the interaction (less than 1%). Each circle is composed of three gray and three blue disks. The total force F_{mb} acting on the tip is then the sum of the individual forces F_{cj} (or F_{sj} depending on the modeling of the tip, point charge or semisphere) acting between one patch and the tip:

$$F_{\mathrm{mbc,s}}(D) = \sum_{j=1}^{N} F_{\mathrm{cj,sj}}(D_j), \text{ where } D_j = \sqrt{({R_{\mathrm{cj}}}^2 + D^2)} \quad (9)$$

Fitting Procedure. The best theoretical fit of the experimental physical plots was obtained by minimizing the nonlinear error χ^2

$$\chi^2 = \min \sum_{i=1}^{n} \left[\frac{(F_{\mathrm{exp}} - F_{\mathrm{calc}})_i^2}{\Gamma_{F,i}} \right] \quad (10)$$

where n is the number of points in the data set, Γ_{Fj} is the error in the measurement estimated to be around 0.1 nN, F_{exp} represents the experimental forces, and F_{calc} is obtained from the theoretical model. The method of Levenberg−Marquardt[27,28] is then used to minimize χ^2.

There were three variable parameters for both models: R − the domain radius of the lipid patch and Q_p or Q_s for the charge of the tip and the tip radius. Therefore, the nonlinear error χ should be minimized with consideration for these parameters, where the domain radius, tip radius, and tip charge corresponding to the minimum nonlinear error χ should be chosen. The radius of the AFM tip was varied between 2 and 30 nm, the surface charge was varied between 10^{-20} and 10^{-16} C, and the radius of the electrostatic domains was varied between 1 and 50 nm. The best fit was obtained by minimizing the nonlinear error χ, when three parameters were varied simultaneously as a 3×3 matrix. Although we varied the radius of the probe, the best fit was found at a radius of 10 nm, as expected for these tips. We used a silicon tip without any modification or applying additional voltage.

Results and Discussion

We reported earlier that BLES functional surfactant films are characterized by the formation of large multilayer structures[7] (5, 10, and up to hundreds of nanometers high) separated from each other (Figure 2A). This multilayer formation is significantly suppressed in the presence of excess cholesterol,[7] and only a monolayer with a few unstructured clusters is observed (Figure 2B).

In addition to these morphological differences, the structure of the monolayer also differs for BLES with and without cholesterol. We imaged flat monolayer areas for both samples with FM-KPFM. In the absence of cholesterol, the monolayer and most of the multilayers are mostly unstructured in potential. Figure 2C shows the topography of the monolayer and part of the bilayer, which are uniform in potential (Figure 2F). On a larger scale over 100 μm^2, some of the multilayers show large variances in potential due to the uneven distribution of surfactant-specific proteins,[29,30] but the monolayer remains flat and uniform in potential. In contrast, films containing 20% cholesterol are relatively flat monolayers with respect to topography (Figure 2D) with deviations in height of less than 1 nm but strongly structured in potential (Figure 2G). FM-KPFM images (Figure 2G) revealed that excess cholesterol induces small (10−50 nm in diameter) electrostatic domains in the surfactant monolayer, which cannot be well resolved by other KPFM modes, for example, lift mode or amplitude-modulation KPFM.[26] The monolayer with 0% cholesterol (Figure 2F) is relatively flat in potential (deviations in potential are less than 10 mV) with an average surface potential of −0.6 V. The presence of 20% cholesterol changes the average surface potential to −0.35 and −0.45 V for two different domains with deviations in potential of 100 mV between the domains (Figure 2G). These two types of domains with potentials of −0.35 and − 0.45 V, schematically presented in Figure 2E, were used in the models.

The presence of these electrostatic domains induced by cholesterol correlates with the effect of lipid condensation induced by cholesterol as reported earlier.[28,29,31] In general, the packing of lipid membrane or monolayer is related to the lipid dipole moments, and may affect the surface potential. It has been shown that the presence of cholesterol in a DPPC bilayer[32] has a strong effect on the membrane dipole potential because of the deeper penetration of water molecules afforded by cholesterol, allowing for a nonzero electric field to penetrate more deeply into the bilayer interior. These findings correlate with our observation of a large variation in the electrical potential distribution in BLES monolayer films, observed with FM-KPFM in the presence of cholesterol.

(27) Marquardt, D. W. *J. Soc. Ind. Appl. Math.* **1963**, *11*, 431–441.
(28) Bevington, P. R. *Data Reduction and Error Analysis for the Physical Sciences*; McGraw-Hill: New York, 1969.
(29) Leonenko, Z.; Rodenstein, M.; Dohner, J.; Eng, L. M.; Amrein, M. *Langmuir* **2006**, *22*, 10135–10139.
(30) Hane, F.; Moores, B.; Amrein, M.; Leonenko, Z. *Ultramicrosc. J.* **2009**, *109*, 968–973.
(31) Mozaffary, H. *Thin Solid Films* **1994**, *244*, 874–877.
(32) Chiu, S. W.; Jakobsson, E. *J. Chem. Phys.* **2001**, *114*, 5435–5443.

When it comes to interactions with charged species, the local changes in surface potential may play an important role because they may regulate the distinctive affinity of some regions over the rest of the film surface. In this work, we focused on the electrical surface potential of the PS film and how it may affect the interaction of the AFM probe with the film's surface. With AFM force spectroscopy, we measured the interaction forces between the AFM probe and the supported BLES monolayer with and without 20% cholesterol. The approach part of the curve was analyzed for electrostatic interaction. In this work, we focused only on the electrostatic force; the elastic deformation of the lipid has not been considered. The van der Waals' forces normally are considerably lower than the electrostatic forces[20,21] (more than 10 times lower as measured in this work); therefore, the van der Waals interactions have been neglected in this study. With atomic force spectroscopy, we showed that the interaction of the AFM probe with the electrical field, arising from the PS monolayer, is affected by the presence of electrostatic domains induced by cholesterol, producing longer-ranged, stronger electrostatic forces. The apex of the AFM probe may serve as a model nanoparticle; therefore, this approach may help to investigate the interaction of nanoparticles with PS films. Figure 2E shows a schematic representation of the electrostatic interaction of the nanoparticle (AFM probe) with electrostatic domains observed by FM-KPFM (Figure 2G).

To analyze the electrostatic part of the interaction, experimental force curves were fit with theoretical models. To account for the nonuniform surface potential distribution that we observed by FM-KPFM, we introduced patches (or domains) of various radii and surface potentials. We considered the AFM probe to interact with this film as (1) a point charge, Q_{tip}, and (2) a semisphere. The force induced on the AFM tip modeled as a point charge is given by eq 5, and the force induced on the AFM tip modeled as a point semisphere is given by eq 8. The experimentally measured electrical surface potential V was used as a parameter in a fitting procedure. The sample with 0% cholesterol was characterized by a surface potential of −0.6 V, determined from the cross-section analysis of FM-KPFM images. For the samples with 20% cholesterol, two potentials were experimentally determined for two different domains: −0.35 and −0.45 V. The domain size R and the AFM tip charge Q_s or Q_{tip} were used as variable parameters to obtain the best fit. We used a silicon tip without any modification or applying additional voltage. From the experimental force plots observed, it was clear that the tip was charged and the electrical field produced by the surface potential of surfactant had a charge of the same sign as the charge on the tip, which leads to repulsion. For 0% cholesterol, the best fit was obtained at a tip charge of 10^{-17}C, and for 20% cholesterol, the best fit was obtained at a tip charge of 10^{-16} C. The tip radius found to give the best fit was at 10 nm in all models. The important finding is that the repulsion between the tip and the film increased because of the presence of 20% cholesterol in the film and because of the presence of a nonuniform potential distribution or nanoscale electrostatic domains induced by cholesterol.

When comparing the point charge to the semisphere model, we found experimentally a ratio of ~10 in the surface charge given by the sphere and the point charge. To understand this, we should compare charges using the effective distance D_{eff} to the patch. One should consider the fact that the semisphere charge is not localized at the very end of the tip but rather in the center of mass of the semisphere, which is located at around $^3/_4$ tip radius away from the tip end (Figure 1C). The effective distance in this case should be enlarged by approximately $\Delta = 3R_s/4$. The force acting on the tip is roughly the ratio of the charge Q_{tip} and the effective D_{eff}^2. Because the effective distance is larger than D for the semisphere model, the semisphere charge Q_s should be larger than the point charge Q_p to fit the experimental force curve.

$$\frac{Q_s}{Q_p} = \frac{(D+\Delta)^2}{D^2} \tag{11}$$

Figure 3 shows the average of experimental force plots and theoretical fits (Figure 3a,c) and the standard deviations (Figure 3b,d). We observed that electrostatic forces were short-range forces (< 5 nm) in the case of a cholesterol-free layer (Figure 3a), whereas the presence of cholesterol (20%) induced a long-range interaction (> 10 nm) (Figure 3c).

Experimental force plots and the theoretical fit for the point charge model and the semisphere model (eqs 5 and 8) are shown in Figure 3a for the BLES sample with 0% cholesterol. Both models fit well with the experimental data and give a small domain radius of around 1.2−3.7 nm. This small domain size corresponds to a patch composed of only a few lipids heads (assuming 2 nm^2 for the gyration area of one lipid). This also corresponds to observations by FM-KPFM of a relatively uniform distribution of surface potential (Figure 2F). Figure 3b shows the dependence of standard deviation (STD) on distance between the tip and the sample. For both models, the standard deviation was small over the distances between 3 and 14 nm. The standard deviation is higher when the tip is close to the contact point.

When using the single domain model for the sample with 0% cholesterol, the best fit was obtained at R = 2.7 nm (Q_{tip} = -1.0×10^{-17} C, V = −0.6 V, and χ = 3.9 when considering the AFM tip to be a point charge), R = 0.74 nm (Q_{tip} = -7×10^{-17} C, V = −0.6 V, and χ = 2.2 when considering the AFM tip to be a semisphere), and R_{tip} = 10 nm. When using the single domain model for a sample with 20% cholesterol, the best fit was obtained at R = 7.4 nm (Q_{tip} = -1.8×10^{-16} C, V = −0.35 to 0.45 V, and χ = 19.8 for a point charge), and with semisphere model, the best fit was obtained at R = 7.4 nm (Q_{tip} = -3.8×10^{-16} C, V = −0.35 to 0.45 V, and χ = 22.4).

Electrostatic forces measured on BLES with a 20% cholesterol sample extend to a wider range of up to 15−20 nm (Figure 3c), compared to 5 nm measured on the sample with 0% cholesterol. In the case of 20% cholesterol, the analysis of the theoretical fit shows an increase in the domain radius of up to 10 times (from 0.74 to 7.4 nm, point charge, single domain model) as well as an increase in the effective charge of the tip when compared to BLES with 0% cholesterol. The larger domain size is consistent with the nonuniform surface potential distribution shown on the KPFM image (Figure 2G), which shows the presence of electrostatic domains with variable radii between 10 and 50 nm. Taking into account the domain size, the radius of the tip, and the long-range nature of the interaction in the case where 20% cholesterol is present in the film, the point charge model generally gives a better fit than the semisphere model (plot C, Figure 3c). We considered the interaction of the tip with the closest single domain right below the tip and assumed that the presence of the AFM tip does not influence the uniform charge distribution on the patch surface. Because of these assumptions, one should expect a discrepancy between model predictions and experimental results over short ranges (where the tip comes into contact and violates the surface charge distribution) as well as over wide ranges (where the presence of neighboring patches should be taken into account). Direct comparison with experimental results showed that with the exception of these two extreme limits (D < 3 nm and D > 14 nm) both proposed models fit the experimental data well, although the range is slightly different for the case with no

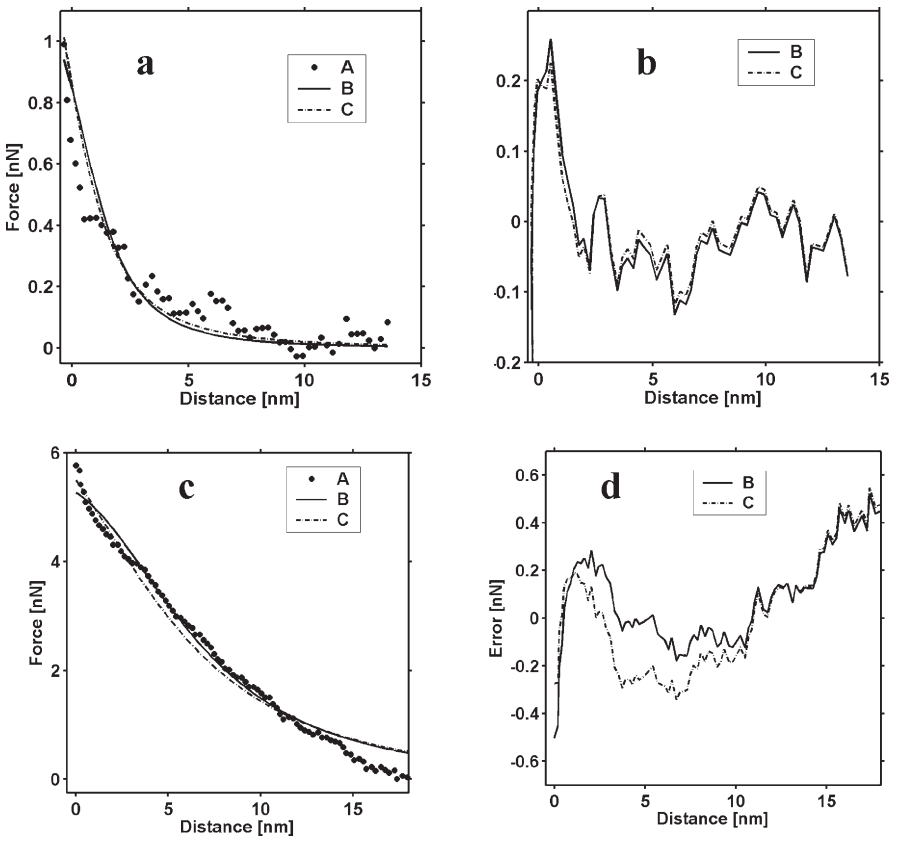

Figure 3. (a) Electrostatic forces measured on a BLES film with 0% of cholesterol, single domain model: (A) experimental data, (B) point charge model fit, and (C) semisphere model fit. (b) Dependence of standard deviation vs distance calculated on BLES film with 0% cholesterol: (B) point charge model fit and (C) semisphere model fit. (c) Electrostatic forces measured on a BLES sample with 20% cholesterol, single domain model: (A) experimental data, (B) point charge model fit, and (C) semisphere model fit. (d) Dependence of standard deviation vs distance calculated on a BLES film with 20% cholesterol: (B) point charge model and (C) semisphere model.

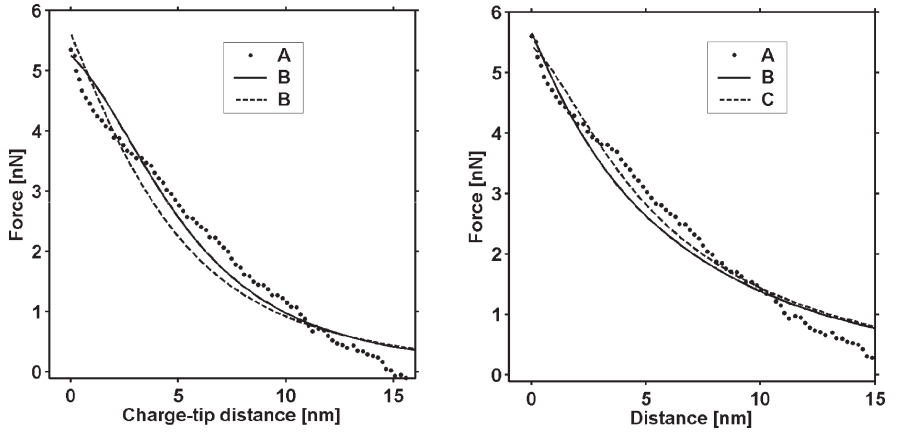

Figure 4. Comparison between the single domain model and multibody model. Electrostatic forces measured on a BLES sample with 20% cholesterol. (Left) Single domain model: (A) experimental data, (B) theoretical fit with the point charge model (best fit at $R = 7.4$ nm; $Q_{tip} = -1.8 \times 10^{-16}$ C, $V = -0.35{-}45$ V, and $\chi = 22.4$), and (C) theoretical fit with the semisphere model (best fit at $R = 7.4$ nm; $Q_{tip} = -3.8 \times 10^{-16}$ C, $V = -3.5{-}0.5$ V, and $\chi = 22.4$). (Right) Multibody model: (A) experimental data, (B) theoretical fit with the point charge model (best fit at $R = 5.36$ nm; $Q_{tip} = -1.1 \times 10^{-16}$ C, $V = -0.35{-}0.45$ V, and $\chi = 10$), (C) theoretical fit with the semisphere model (best fit at $R = 4$ nm; $Q_{tip} = -3.16 \times 10^{-16}$ C, $V = -0.35{-}0.45$ V, and $\chi = 12.6$).

cholesterol (2 nm $< D <$ 15 nm) and for the case with excess cholesterol (3 nm $< D <$ 14 nm), which is a result of different patch sizes for these samples. Results of the fit using the multibody model are comparable with a single domain model in the 2−15 nm range, (Figure 4), showing that the single domain and the point charge models give better correlation with the radius of domains obtained by FM-KPFM surface potential imaging.

What is important is that all models give consistent results, indicating the smaller domain radius in the case of 0% cholesterol compared to the sample with 20% cholesterol. The theoretical fit for 20% cholesterol using these models gives a domain radius that

is up to 10-fold larger than that obtained for a sample with 0% cholesterol. These findings correlate well with the experimentally observed larger domains in the sample with 20% cholesterol and the relatively flat surface potential image observed for 0% cholesterol (Figure 2F,G).

In summary, the models we used fit well with the experimental force plots gathered, showing the presence of electrostatic interactions in the net force measured between the tip and the sample. Samples of BLES with 20% cholesterol exhibit stronger electrostatic repulsion at longer distances, compared to samples with 0% cholesterol, for all models used when interacting with the AFM tip. The experimental data and theoretical fit both revealed that the size of the domains is up to 10 times larger for the film containing 20% cholesterol than that with no cholesterol present. These findings reveal the important role of cholesterol in changing the electrical surface potential of the PS film and producing electrostatic domains, which cause an increase in the total electrostatic force. Our experimental data correlate with the results of molecular dynamics simulations[32] where cholesterol was shown to order individual lipids adjacent to cholesterol molecules, cause the long-range cooperativity between lipids to vanish, and alter the lipid electrostatic potential[33] In the DPPC bilayer, it was shown that the membrane electrostatic potential in the presence of cholesterol[33] has a much larger variance depending on the distance along the bilayer normal, as compared to the pure bilayer.

(33) Israelachvili, J. N. *Intermolecular and Surface Forces*, 2nd ed.; Academic Press: London, 1991.

Conclusions

This example of our application of FM-KPFM and force measurements to study a pulmonary surfactant illustrates a key point of central importance: that novel high-resolution imaging techniques such as FM-KPFM, which sense electrostatic forces, are suitable for studying electrostatic properties of biological samples on the nanoscale. With FM-KPFM imaging and force measurements, we revealed a previously unknown effect of cholesterol to influence the local electric fields around PS films and change the electrostatic interaction with an AFM probe. This may lead to a new understanding of the mechanism of surfactant function as well as how the charged species may interact with PS films. Electrostatic interactions are driving forces in many biological processes. Knowing the nanoscale electrical surface potential in biofilms is a crucial function-related parameter without which an important link between the function of the biofilm in vivo and its possible pathologies would be missed.

Acknowledgment. This collaborative research has been supported by the Canada Foundation for Innovation, the Natural Sciences and Engineering Research Council of Canada, the Canadian Institute of Health Research, and the University of Burgundy, Dijon, France. We are grateful to BLES Biochemicals Inc, London, Ontario, for generously providing BLES and JPK Instruments and NIMA for their technical support. We also thank Dr. S. Patchkovskii for critically reading the manuscript and helpful discussions.